High temperature thermoelectric properties of the tetradymite Bi2–xPbxTe2Se ($0 \leq x \leq 0.03$)

Adèle Léon, Shantanu Misra, Petr Levinský, Jiří Hejtmánek, Bartlomiej Wiendlocha, Bertrand Lenoir, Christophe Candolfi

Applied Physics Letters

High temperature thermoelectric properties of the tetradymite $Bi_{2-x}Pb_xTe_2Se$ ($0 \leq x \leq 0.03$)

Cite as: Appl. Phys. Lett. **119**, 232103 (2021); https://doi.org/10.1063/5.0077166
Submitted: 31 October 2021 • Accepted: 24 November 2021 • Published Online: 08 December 2021

Adèle Léon, Shantanu Misra, Petr Levinský, et al.

AIP Publishing

Applied Physics Letters ARTICLE scitation.org/journal/apl

High temperature thermoelectric properties of the tetradymite $Bi_{2-x}Pb_xTe_2Se$ ($0 \leq x \leq 0.03$)

Cite as: Appl. Phys. Lett. **119**, 232103 (2021); doi: 10.1063/5.0077166
Submitted: 31 October 2021 · Accepted: 24 November 2021 ·
Published Online: 8 December 2021

Adèle Léon,[1] Shantanu Misra,[1] Petr Levinský,[2] Jiří Hejtmánek,[2] Bartlomiej Wiendlocha,[3] Bertrand Lenoir,[1,a)] and Christophe Candolfi[1,a)]

AFFILIATIONS

[1]Institut Jean Lamour, UMR 7198 CNRS–Université de Lorraine, Campus ARTEM, 2 allée André Guinier, BP 50840, 54011 Nancy, France
[2]FZU–Institute of Physics of the Czech Academy of Sciences, Cukrovarnická 10/112, 162 00 Prague 6, Czech Republic
[3]Faculty of Physics and Applied Computer Science, AGH University of Science and Technology, Al. Mickiewicza 30, 30-059 Krakow, Poland

Note: This paper is part of the APL Special Collection on Thermoelectric Materials Science and Technology Towards Applications.
[a)]**Authors to whom correspondence should be addressed:** bertrand.lenoir@univ-lorraine.fr and christophe.candolfi@univ-lorraine.fr

ABSTRACT

We report on the synthesis, characterizations, and high-temperature thermoelectric properties of polycrystalline samples of $Bi_{2-x}Pb_xTe_2Se$ for $0 \leq x \leq 0.03$. Powder x-ray diffraction and scanning electron microscopy confirm the successful insertion of Pb into the hexagonal unit cell of the tetradymite Bi_2Te_2Se. Pb acts as an acceptor-like impurity, gradually shifting the lightly doped, *n*-type electronic properties of Bi_2Te_2Se toward heavily doped, *p*-type properties in Pb-containing samples, which is additionally confirmed by electronic structure calculations. The increased degenerate character results in high power factors while maintaining low thermal conductivity values. This favorable combination of thermoelectric properties yields a peak dimensionless figure of merit ZT of 0.70 at 425 K for $x = 0.02$ in the direction perpendicular to the pressing direction.

In the absence of greenhouse gas emissions or moving parts, thermoelectric devices enable a direct solid-state conversion between heat and electricity or vice versa that provides a sustainable mean for power generation or cooling.[1–4] The conversion efficiency of thermoelectric materials is primarily quantified by the dimensionless thermoelectric figure of merit ZT defined as $ZT = \alpha^2 T/\rho(\kappa_e + \kappa_L)$, where α is the thermopower or Seebeck coefficient, T is the absolute temperature, ρ is the electrical resistivity, and κ_e and κ_L are the electronic and lattice thermal conductivity, respectively.[1,2] Because these transport coefficients are mutually interdependent through the carrier concentration, narrow-bandgap semiconductors with a complex crystal structure show the best compromise between good electronic and poor thermal properties.[1–5]

Tetradymites are a class of naturally occurring materials of general chemical formula M_2X_3, where M is a pnictogen (Bi, Sb, or As) and X is a chalcogen element (Te, Se, or S), which fulfill the above-mentioned requirements. These phases, which belong to homologous series,[6,7] crystallize in a rhombohedral structure (space group $R\bar{3}m$ or $P\bar{3}m1$) built by atomic layers stacked along the *c*-axis forming a sequence of quintuple layers separated by van der Waals gaps. Their electronic properties are characterized by small bandgaps and effective masses and strong spin–orbit coupling,[8–10] making them a prospective area of research to design highly efficient thermoelectric materials for near-room-temperature applications and topological insulators.[11–13] A key property of these compounds is the small difference in electronegativity between the M and X atoms that favors the formation of antisite defects or vacancies.[14–16] Because this inherent defect chemistry is particularly sensitive to the synthesis route, a careful control of the stoichiometry is difficult to achieve experimentally. Depending on the nature and concentration of the dominant defects, both heavily doped *n*- or *p*-type compounds can be obtained.[17,18]

As a representative of the full solid solution between Bi_2Se_3 and Bi_2Te_3,[19,20] the ternary Bi_2Te_2Se stands out due to its crystallographically ordered structure that results from the preferential occupation of Se in the central layer of the quintuple sequence. In contrast to the doubly positively charged Se vacancies and singly ionized Bi_{Te} antisite defects that dominate in Bi_2Se_3 and Bi_2Te_3, respectively, the defect scheme in Bi_2Te_2Se is more complex. Charge-neutral Se_{Te} and Te_{Se}

antisite defects have been proposed to coexist with Bi_{Te} antisite defects and Te vacancies giving holes and electrons, respectively.[21] This compensation can lead to a bulk insulating behavior with carrier densities as low as 8×10^{14} cm^{-3} upon Sn doping,[22–25] a favorable characteristic to study its topological surface states.[26,27] The delicate balance between hole-like and electron-like properties can be tipped to achieve either *n*- or *p*-type electrical conduction.[28–31] While the influence of *n*- or *p*-type dopants on the thermoelectric properties of various tetradymites has been the subject of numerous studies,[32–36] the possibility to introduce aliovalent acceptor impurities in Bi_2Te_2Se has not been considered experimentally to date.

Here, we report on the synthesis of polycrystalline $Bi_{2-x}Pb_xTe_2Se$ samples and investigate the influence of Pb on the high-temperature thermoelectric properties. Our results evidence that Pb acts as an acceptor impurity, driving the nondegenerate, *n*-type electronic properties of Bi_2Te_2Se toward degenerate *p*-type behavior. This *n*-to-*p*-type transition is supported by first-principles calculations of the density of states (DOS) of the studied material containing Pb and *n*-type defects. The combination of low lattice thermal conductivity κ_L and enhanced power factor $PF = \alpha^2/\rho$ yields a peak ZT value of 0.70 at 420 K for $x = 0.02$ in the direction perpendicular to the pressing direction. The experimental and computational methods are presented in the supplementary material. Hereafter, only measurements performed in the direction perpendicular to the pressing direction, that is in the direction along which the thermoelectric performance is the highest, are presented. Measurements carried out in the parallel direction are shown in Fig. S1 of the supplementary material.

Regardless of the Pb content, the powder x-ray diffraction (PXRD) patterns can be fully indexed with the rhombohedral crystal structure of Bi_2Te_2Se described in the space group $R\bar{3}m$ (Fig. 1). Up to $x = 0.02$, no secondary phases are detected within the detection limit

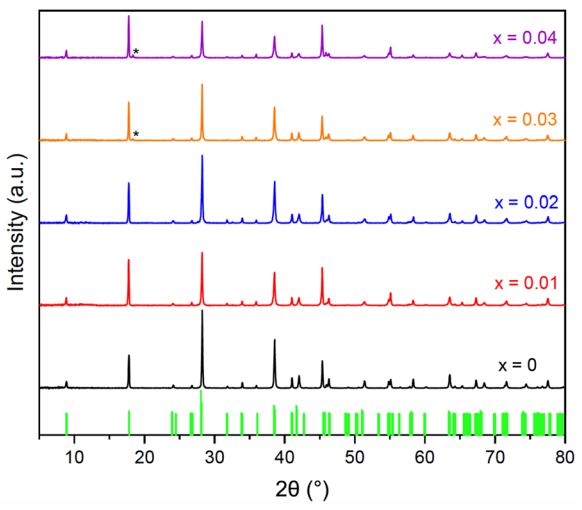

FIG. 1. Powder x-ray diffraction patterns of the series $Bi_{2-x}Pb_xTe_2Se$ for $0.0 \leq x \leq 0.04$. The theoretical PXRD pattern is also shown for comparison. The asterisks mark the unidentified secondary phase (see Figs. S2 and S3 in the supplementary material for SEM images of the $x = 0.03$ and 0.04 samples). Note that the anisotropic crystal structure of these compounds tends to result in the preferential orientation of the crystallites, giving rise to the observed renormalization of the relative intensities of the peaks.

of this technique. Their absence is further confirmed by SEM images along with their corresponding x-ray maps (Fig. S2 in the supplementary material), indicating a homogeneous distribution of the four elements. Traces of a secondary phase become visible on the patterns of the $x = 0.03$ and 0.04 samples, the nature of which could not be unequivocally determined from this single reflection. Although no obvious secondary phase could be directly observed on the x-ray mapping images, slight inhomogeneities in the spatial distribution of the elements appear for $x = 0.04$ (Fig. S3 in the supplementary material). These results suggest a solubility limit of Pb lying between both compositions despite their similar transport properties (Fig. S4 in the supplementary material). The unit cell volume, calculated from the lattice parameters determined from Rietveld refinements against the PXRD data, increases with increasing x (Fig. S5 in the supplementary material). The negative pressure exerted by Pb on the unit cell is consistent with the larger atomic radius of Pb (175 pm) compared to Bi (154.5 pm), further confirming the successful substitution of Pb for Bi in Bi_2Te_2Se.

Figures 2(a) and 2(b) show the temperature dependence of the electrical resistivity ρ and thermopower α measured in the direction perpendicular to the pressing direction for $Bi_{2-x}Pb_xTe_2Se$ ($0.0 \leq x \leq 0.03$). In agreement with literature data,[15,24–31] the pristine sample behaves as a *n*-type heavily doped semiconductor with room-temperature ρ and α values of 30 $\mu\Omega$ m and 230 μV K^{-1}, respectively. Upon warming, Bi_2Te_2Se enters an intrinsic regime of conduction above 400 K evidenced by decreasing ρ and $|\alpha|$ values due to the thermal activation of minority carriers across the bandgap. The substitution of Pb for Bi leads to a crossover to a *p*-type electrical conduction with ρ and α values decreasing with increasing x up to $x = 0.03$ at 300 K. These results show that Pb acts as an acceptor impurity in Bi_2Te_2Se driving its *n*-type character toward *p*-type electrical property characteristics of heavily doped semiconductors.

The *n*-to-*p*-type crossover upon Pb doping is well reproduced in our electronic structure calculations using the Korringa-Kohn-Rostoker method with the coherent potential approximation (KKR-CPA)[37–39] illustrated in Fig. 3. In Fig. 3(a), the electronic density of states is calculated for $Bi_2Te_{1.998}Se$, i.e., containing 0.1% of Te vacancies. Such a concentration of vacancies corresponds to an *n*-type compound with $n = 2.5 \times 10^{19}$ cm^{-3}, close to that observed in our samples with the Fermi level E_F being located near the bottom of the conduction band. When such a system is doped with Pb, a concentration as low as $x = 0.01$ is sufficient to induce an *n*-to-*p*-type transition [Fig. 3(b)]. Upon increasing the Pb concentration, the Fermi level is shifted deeper into the valence bands. Such behavior is similar to what was observed for Mg- or Ca-doped tetradymites initially containing donor-like vacancies.[40] From the partial Pb DOS plotted in Fig. 3, we further expect that, in the investigated doping range, the properties of the Pb-doped samples should approximately follow a rigid-band-like trend, as the partial Pb DOS near the band edge is similar to that of Bi with a small enhancement of DOS seen deeper at ~0.5 eV below E_F.

The maxima in $|\alpha|$ and ρ for Bi_2Te_2Se are shifted toward higher temperatures upon Pb doping from 450 and 500 K for $x = 0.01$ to 500 and 600 K for $x \geq 0.01$, respectively. The maximum α value of the $x = 0.0$ sample ($\alpha_{max} = -237$ μV K^{-1}) and the corresponding temperature ($T_{max} = 380$ K) were used to estimate the bandgap energy E_g using the Goldsmid–Sharp relation $E_g = 2e\alpha_{max}T_{max}$,[41] where e is the elementary charge. The E_g value of 288 meV is in excellent agreement

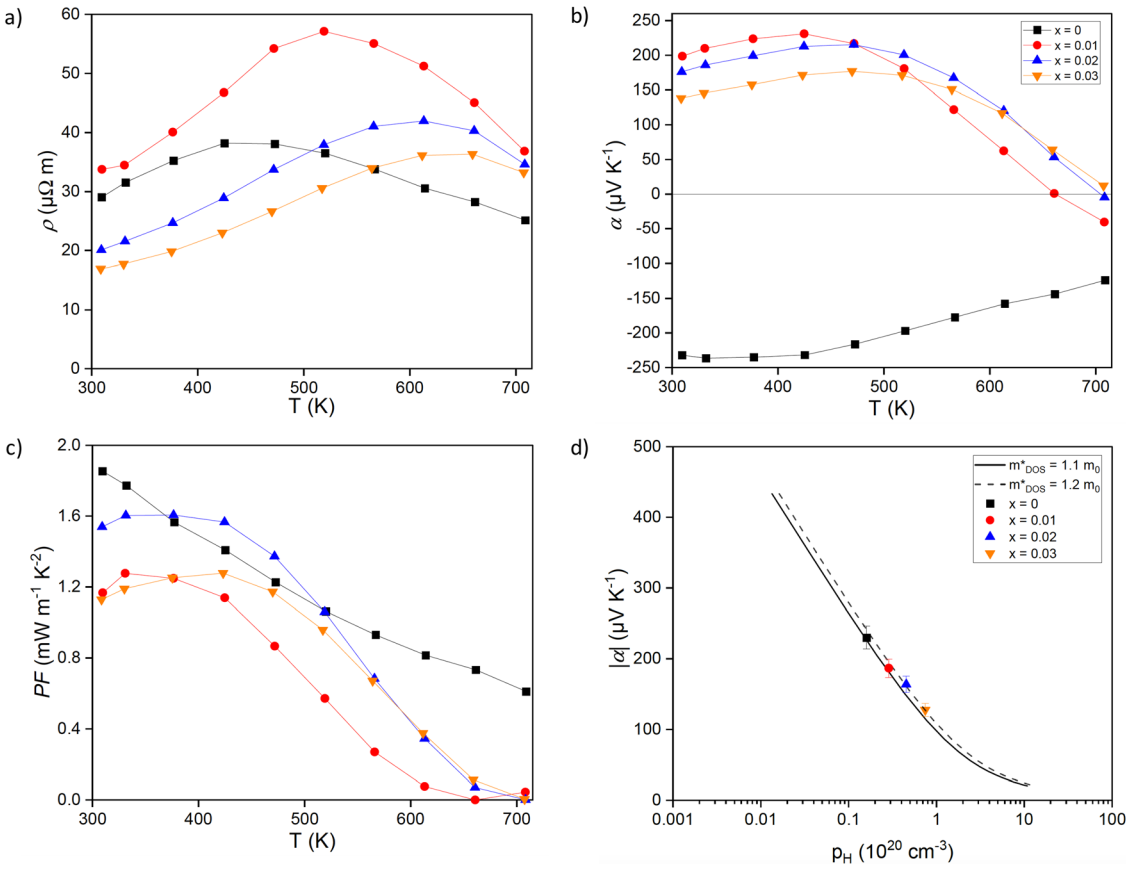

FIG. 2. Temperature dependence of (a) the electrical resistivity ρ, (b) the thermopower α, (c) the power factor $PF = \alpha^2/\rho$, and (d) the Ioffe–Pisarenko plot at 300 K of the series $Bi_{2-x}Pb_xTe_2Se$ for $0.0 \leq x \leq 0.03$. Only the data measured perpendicular to the pressing direction are shown. The color-coded symbols are similar for panels (a)–(c). In panel (d), the solid and dashed curves represent the theoretical $\alpha(p)$ dependence calculated using the single-parabolic band (SPB) model. The vertical error bars correspond to the experimental uncertainty estimated to be 7% for thermopower measurements.

with the experimental values inferred from optical absorption spectroscopy ($E_g = 280$ meV),[8] angle-resolved photoemission spectroscopy (ARPES) ($E_g = 300$ meV)[26] and from the trend in E_g determined for Bi_2Te_3–Bi_2Se_3 alloys.[8,12]

Due to the thermal activation of minority carriers above 400 K, the power factor PF reaches its peak value around this temperature for all Pb-doped samples [Fig. 2(c)]. The decrease in α with increasing Pb content is not counterbalanced by the concomitant decrease in ρ leading to lower PF values at 300 K with respect to the pristine sample. Nevertheless, the high values characterizing the $x = 0.02$ sample (1.55 mW m^{-1} K^{-2} at 300 K) are maintained up to about 425 K, eventually surpassing those of the ternary compound between 400 and 500 K. These values remain, nevertheless, lower than those achieved in optimally doped p-type Bi_2Te_3 near room temperature (3.5 mW m^{-1} K^{-2}).[12]

In agreement with the α data, the sign of the Hall coefficient R_H confirms the crossover from n- to p-type electrical properties upon Pb doping (Fig. S6 in the supplementary material). The electron concentration n_H of 1.7×10^{19} cm^{-3} for the $x = 0.0$ sample is similar to the densities reported in several prior studies for polycrystalline and single-crystalline Bi_2Te_2Se.[15,24–30,36,42–44] In the Pb-doped samples, the hole concentration p_H increases at 300 K to reach 7.5×10^{19} cm^{-3} for $x = 0.03$. The values of the electron mobility μ_H remain relatively high for Bi_2Te_2Se, reaching 71 and 122 cm^2 V^{-1} s^{-1} at 300 K in the parallel and perpendicular directions, respectively. The substitution of Pb for Bi enhances point-defect scattering, leading to an overall decrease in the hole mobility values that eventually reach 52 cm^2 V^{-1} s^{-1} at 300 K for $x = 0.03$ in the perpendicular direction.

The effect of Pb doping on the α values at 300 K was further analyzed using the Ioffe–Pisarenko representation [Fig. 2(d)]. The theoretical $\alpha(p_H)$ dependence was calculated using a single-parabolic band (SPB) model with acoustic phonon scattering. This model is expected to provide a reasonable description of the conduction band minimum in lightly doped, n-type Bi_2Te_3 and Bi_2Se_3 (for $\sim 1 \times 10^{19}$ cm^{-3}) for which the Fermi surface is composed of six small interconnected ellipsoidal pockets and a single, slightly elongated ellipsoidal pocket centered at the Γ point of the Brillouin zone, respectively.[11,12] In contrast, the Fermi surface in p-type Bi_2Te_3 is more complex with a flower-like structure composed of six strongly elongated, disconnected ellipsoidal hole pockets (for $\sim 1 \times 10^{19}$ cm^{-3}).[11,12] The density-of-states effective mass m^*_{DOS} values derived for p-type compounds should, therefore, be taken with some caution but nevertheless allow for a direct comparison of tetradymite of various compositions.[12] For pristine n-type Bi_2Te_2Se, the m^*_{DOS}

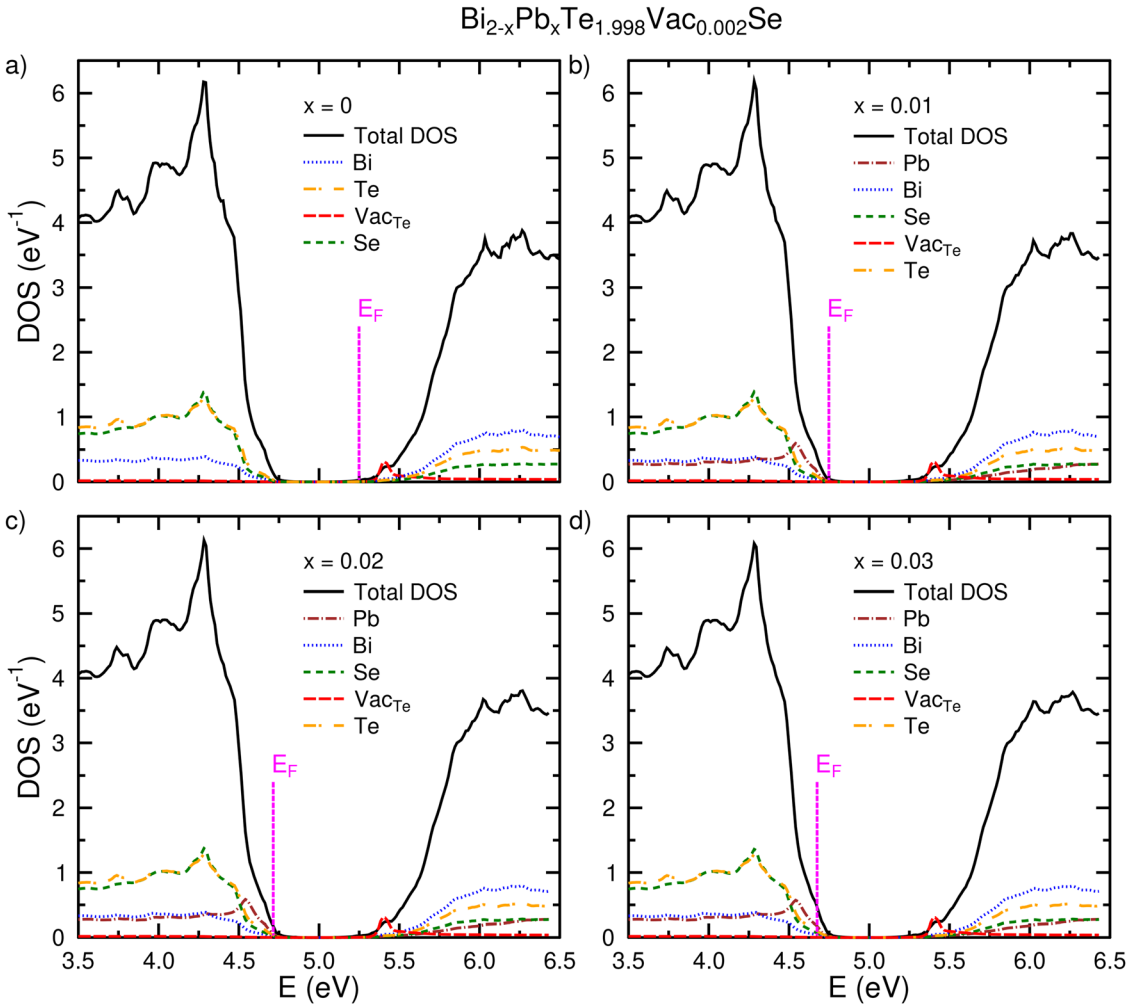

FIG. 3. Evolution of the electronic density of states (DOS) of $Bi_2Te_{1.998}Se$ (containing 0.002 of Te vacancies per formula unit) upon doping with Pb. The *n*-to-*p*-type crossover is observed as the Fermi level E_F changes the location from the bottom of conduction bands to the top of the valence bands.

of 1.1 m_0 (m_0 is the free electron mass) inferred from the SPB model is equivalent to that estimated for *n*-type Bi_2Te_3 (1.06 m_0). The weak influence of Se on the shape of the conduction band edge is in line with the fact that the conduction manifold in Bi_2Te_3 mostly derives from Bi *p*-states.[12] The m^*_{DOS} of 1.2 m_0 inferred for the Pb-doped samples is slightly higher than that estimated for the valence band edge of Bi_2Te_3 (1.06 m_0).[12] The good agreement between the theoretical and experimental $\alpha(p_H)$ dependences is consistent with our theoretical calculations predicting that Pb should behave as a rigid-like impurity in Bi_2Te_2Se over the carrier concentration range covered.

As useful parameters for comparing the thermoelectric performance of Bi_2Te_2Se with its parent compound Bi_2Te_3, the weighed mobility μ_w and thermoelectric quality factor B were calculated using the relations[45–48]

$$\mu_w = \mu_0 \left(\frac{m^*_{DOS}}{m_0}\right)^{3/2}, \quad (1)$$

$$B = \left(\frac{k_B}{e}\right)^2 \frac{8\pi e (2m_0 k_B)^{3/2}}{h^3} \frac{\mu_w T^{5/2}}{\kappa_L}, \quad (2)$$

where μ_0 is the intrinsic hole mobility calculated from the SPB model, k_B is the Boltzmann constant, e is the elementary charge, h is the Planck constant, and κ_L is the lattice thermal conductivity (see below). μ_w, which quantitatively characterizes the power factor at a given doping level and temperature, directly determines B, which provides valuable information regarding the peak ZT value achievable upon doping. At 300 K, these two relations yield $\mu_w = 151\ cm^2\ V^{-1}\ s^{-1}$ and $B = 0.12$, which decrease to $79\ cm^2\ V^{-1}\ s^{-1}$ and 0.06, respectively, for the $x = 0.03$ sample. These lower values compared to *p*-type Bi_2Te_3 ($\mu_w = 400\ cm^2\ V^{-1}\ s^{-1}$ and $B = 0.20$)[12] can be attributed to enhanced point-defect scattering caused by Se for Te and Pb for Bi substitutions, a detrimental impact which is not counterbalanced by the concomitant decrease in κ_L discussed hereafter.

The temperature dependence of the total thermal conductivity κ is shown in Fig. 4(a). Regardless of the Pb content, all samples show

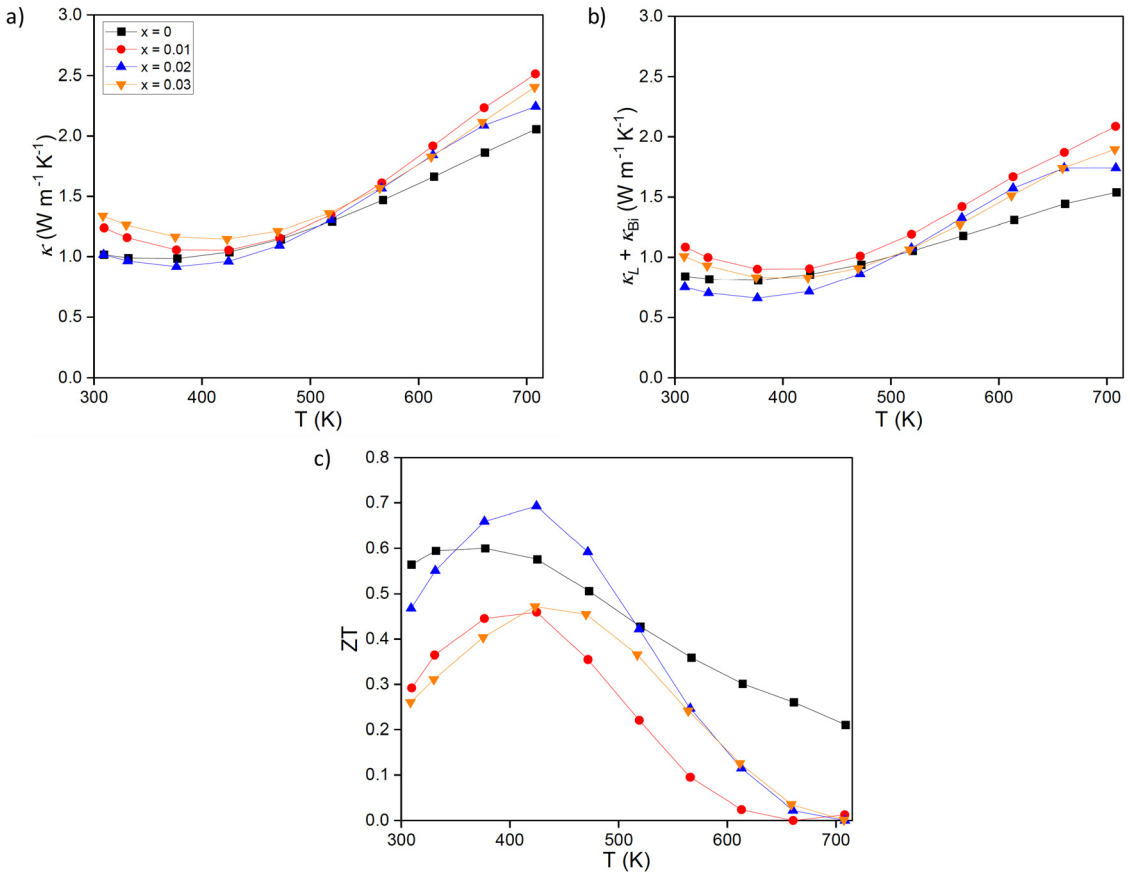

FIG. 4. Temperature dependence of (a) the total thermal conductivity κ, (b) the sum of the lattice thermal conductivity κ_L and the bipolar contribution κ_{Bi}, and (c) the dimensionless thermoelectric figure of merit ZT of the series $Bi_{2-x}Pb_xTe_2Se$ for $0.0 \leq x \leq 0.03$. The color-coded symbols are similar in all panels. Only the data measured perpendicular to the pressing direction are shown.

low κ values, ranging between 1.0 and 1.3 W m^{-1} K^{-1} at 300 K. With the increasing temperature, κ first reaches a minimum near 400 K before increasing monotonically with temperature up to 700 K. This turnover is due to the contribution of minority carriers that lead to an additional bipolar contribution κ_{Bi}. The electronic thermal conductivity κ_e was determined using the Wiedemann–Franz law $\kappa_e = LT/\rho$, where the temperature dependence of the Lorenz number L was estimated by the SPB model. At 300 K, the lattice thermal conductivity κ_L for the $x = 0.0$ sample is equal to 1.1 W m^{-1} K^{-1} and decreases to 0.75 W m^{-1} K^{-1} for $x = 0.02$ [Fig. 4(b)]. The enhanced disorder associated with Pb doping and the size mismatch between Se and Te that locally distorts the lattice, a feature that has been suggested to modify the lattice vibrations of these alloys by Raman spectroscopy,[49] contribute to lower κ_L. The increase observed above 400 K is an artifact stemming from the bipolar contribution experienced by all the samples with the data reflecting the sum $\kappa_L + \kappa_{Bi}$. This effect leads to strong deviations of the Lorenz number from the values determined by the SPB model and hence to an underestimated contribution of the charge carriers to the thermal transport in this regime.[50]

While the substitution of Se for Te is detrimental to maintaining the high μ_W values characterizing p-type Bi_2Te_3, it contributes to decrease the κ_L values below those measured in the parent compound. This effect is mainly responsible for the high ZT values achieved at 300 K in the $x = 0.0$ and 0.02 samples [Fig. 4(c)]. Upon warming, a peak ZT value of 0.70 at 425 K is achieved in the $x = 0.02$ sample, which remains lower than those obtained in optimally doped p-type Bi_2Te_3 near room temperature.[12,51]

In summary, the influence of substituting Pb for Bi on the thermoelectric properties of the tetradymite Bi_2Te_2Se was studied between 300 and 700 K. The solubility limit of Pb was found to lie between $x = 0.03$ and $x = 0.04$ according to PXRD and SEM analyses. In agreement with first-principles calculations, the n-type electronic properties of Bi_2Te_2Se are driven toward p-type properties upon Pb doping, evidencing that Pb acts as an acceptor-like impurity in this compound. The high thermopower combined with relatively low electrical resistivity result in high power factors with a maximum value of 1.55 mW m^{-1} K^{-2} achieved at 400 K for $x = 0.02$. This composition shows the highest thermoelectric performance with a peak ZT value of 0.70 at 425 K.

See the supplementary material for the experimental and computational methods and for Figs. S1–S6 showing a comparison of the transport properties measured along both directions, the temperature

dependences of one additional sample $x = 0.04$, SEM images, variations in the unit cell volume with x, and the magnetic field dependence of the transverse electrical resistivity.

P.L. and J.H. acknowledge the financial support of the Czech Science Foundation (Project No. 18-12761S). Experiments were performed at MGML (mgml.eu), which was supported within the program of Czech Research Infrastructures (Project No. LM2018096).

AUTHOR DECLARATIONS

Conflicts of Interest

The authors have no conflicts to disclose.

DATA AVAILABILITY

The data that support the findings of this study are available within the article and its supplementary material.

REFERENCES

[1]D. M. Rowe, *Thermoelectrics and its Energy Harvesting* (CRC Press, Boca Raton, FL, 2012).
[2]H. J. Goldsmid, *Thermoelectric Refrigeration* (Springer, New York, 1964).
[3]L. E. Bell, Science **321**, 1457–1461 (2008).
[4]I. Petsagkourakis, K. Tybrandt, X. Crispin, I. Ohkubo, N. Satoh, and T. Mori, Sci. Tech. Adv. Mater. **19**, 836–862 (2018).
[5]G. Tan, L.-D. Zhao, and M. G. Kanatzidis, Chem. Rev. **116**, 12123 (2016).
[6]J. W. G. Bos, H. W. Zandbergen, M.-H. Lee, N. P. Ong, and R. J. Cava, Phys. Rev. B **75**, 195203 (2007).
[7]H. Lind, S. Lidin, and U. Häussermann, Phys. Rev. B **72**, 184101 (2005).
[8]D. L. Greenaway and G. Harbeke, J. Phys. Chem. Solids **26**, 1585–1604 (1965).
[9]M. Z. Mohyedin, M. F. M. Taib, A. Radzwan, A. Shaari, M. Mustaffa, B. U. Haq, and M. Z. A. Yahya, Comput. Theor. Chem. **1182**, 112851 (2020).
[10]S. Lee and P. Allmen, Appl. Phys. Lett. **88**, 022107 (2006).
[11]J. P. Heremans, R. J. Cava, and N. Samarth, Nat. Rev. Mater. **2**, 17049 (2017).
[12]I. T. Witting, T. C. Chasapis, F. Ricci, M. Peters, N. A. Heinz, G. Hautier, and G. J. Snyder, Adv. Electron. Mater. **5**, 1800904 (2019).
[13]D. A. Wright, Nature **181**, 834–834 (1958).
[14]D. O. Scanlon, P. D. C. King, R. P. Singh, A. de la Torre, S. McK. Walker, G. Balakrishnan, F. Baumberger, and C. R. A. Catlow, Adv. Mater. **24**, 2154–2158 (2012).
[15]S. Jia, H. Beidenkopf, I. Drozdov, M. K. Fuccillo, J. Seo, J. Xiong, N. P. Ong, A. Yazdani, and R. J. Cava, Phys. Rev. B **86**, 165119 (2012).
[16]C. Drasar, P. Lostak, and C. Uher, J. Electron. Mater. **39**, 2162–2164 (2010).
[17]G. R. Miller and C.-Y. Li, J. Phys. Chem. Solids **26**, 173–177 (1965).
[18]M. Goto, M. Sasaki, Y. Xu, T. Zhan, Y. Isoda, and Y. Shinohara, Appl. Surf. Sci. **407**, 405–411 (2017).
[19]O. B. Sokolov, S. Ya. Skipidarov, N. I. Duvankov, and G. G. Shabunina, Inorg. Mater. **43**, 8–11 (2007).
[20]M. B. Babanly, E. V. Chulkov, Z. S. Aliev, A. V. Shevelkov, and I. R. Amiraslanov, Russ. J. Inorg. Chem. **62**, 1703–1729 (2017).
[21]L.-L. Wang, M. Huang, S. Thimmaiah, A. Alam, S. L. Bud'ko, A. Kaminski, T. A. Lograsso, P. Canfield, and D. D. Johnson, Phys. Rev. B **87**, 125303 (2013).
[22]J. Xiong, A. C. Petersen, D. Qu, Y. S. Hor, R. J. Cava, and N. P. Ong, Physica E **44**, 917–920 (2012).
[23]J. Nayak, G. H. Fecher, S. Ouardi, C. Shekhar, C. Tusche, S. Ueda, E. Ikenaga, and C. Felser, Phys. Rev. B **98**, 075206 (2018).
[24]Z. Ren, A. A. Taskin, S. Sasaki, K. Segawa, and Y. Ando, Phys. Rev. B **82**, 241306 (2010).
[25]J. Xiong, Y. Luo, Y. Khoo, S. Jia, R. J. Cava, and N. P. Ong, Phys. Rev. B **86**, 045314 (2012).
[26]S. K. Kushwaha, Q. D. Gibson, J. Xiong, I. Pletikosic, A. P. Weber, A. V. Fedorov, N. P. Ong, T. Valla, and R. J. Cava, J. Appl. Phys. **115**, 143708 (2014).
[27]Z. Ren, A. A. Taskin, S. Sasaki, K. Segawa, and Y. Ando, Phys. Rev. B **85**, 155301 (2012).
[28]J.-L. Mi, M. Bremholm, M. Bianchi, K. Borup, S. Johnsen, M. Søndergaard, D. Guan, R. C. Hatch, P. Hofmann, and B. B. Iversen, Adv. Mater. **25**, 889–893 (2013).
[29]M. K. Fuccillo, S. Jia, M. E. Charles, and R. J. Cava, J. Electron. Mater. **42**, 1246–1253 (2013).
[30]S. Jia, H. Ji, E. Climent-Pascual, M. K. Charles, J. Xiong, N. P. Ong, and R. J. Cava, Phys. Rev. B **84**, 235206 (2011).
[31]B.-S. Kim, G. Lee, H.-J. Lim, J. Jang, J. E. Lee, B.-K. Min, S.-J. Joo, S. Park, B.-K. Ryu, and H. S. Lee, J. Electron. Mater. **49**, 5308–5316 (2020).
[32]T. Plecháček, J. Navrátil, J. Horák, and P. Lošták, Philos. Mag. **84**, 2217–2228 (2004).
[33]Y. S. Hor, A. Richardella, P. Roushan, Y. Xia, J. G. Checkelsky, A. Yazdani, M. Z. Hasan, N. P. Ong, and R. J. Cava, Phys. Rev. B **79**, 195208 (2009).
[34]Z. Wang, T. Lin, P. Wei, X. Liu, R. Dumas, K. Liu, and J. Shi, Appl. Phys. Lett. **97**, 042112 (2010).
[35]Y. H. Choi, N. H. Jo, K. J. Lee, H. W. Lee, Y. H. Jo, J. Kajino, T. Takabatake, K.-T. Ko, J.-H. Park, and M. H. Jung, Appl. Phys. Lett. **101**, 152103 (2012).
[36]L.-L. Wang and D. D. Johnson, Phys. Rev. B **83**, 241309(R) (2011).
[37]A. Bansil, S. Kaprzyk, P. E. Mijnarends, and J. Tobola, Phys. Rev. B **60**, 13396 (1999).
[38]T. Stopa, S. Kaprzyk, and J. Tobola, J. Phys.: Condens. Matter **16**, 4921 (2004).
[39]S. Kaprzyk and A. Bansil, Phys. Rev. B **42**, 7358 (1990).
[40]B. Wiendlocha, J. Electron. Mater. **45**, 3515 (2016).
[41]H. J. Goldsmid and J. W. Sharp, J. Electron. Mater. **28**, 869–872 (1999).
[42]N. T. Hung, A. R. T. Nugraha, and R. Saito, Nano Energy **58**, 743–749 (2019).
[43]Y. Tian, G. B. Osterhoudt, S. Jia, R. J. Cava, and K. S. Burch, Appl. Phys. Lett. **108**, 041911 (2016).
[44]N. Fuschillo, J. N. Bierly, and F. J. Donahoe, J. Phys. Chem. Solids **8**, 430–433 (1959).
[45]G. J. Snyder, A. H. Snyder, M. Wood, R. Gurunathan, B. H. Snyder, and C. Niu, Adv. Mater. **32**, 2001537 (2020).
[46]G. D. Mahan, Solid State Phys. **51**, 81–157 (1998).
[47]G. D. Mahan, J. Appl. Phys. **65**, 1578–1583 (1989).
[48]R. P. Chasmar and R. Stratton, Int. J. Electron. **7**, 52–72 (1959).
[49]M. Hong, T. C. Chasapis, Z. G. Chen, L. Yang, M. G. Kanatzidis, G. J. Snyder, and J. Zou, ACS Nano **10**, 4719 (2016).
[50]Ö. Ceyda Yelgel and G. P. Srivastava, Phys. Rev. B **85**, 125207 (2012).
[51]V. Ohorodniichuk, S. El-Oualid, A. Dauscher, C. Candolfi, P. Masschelein, S. Migot, P. Dalicieux, P. Baranek, and B. Lenoir, J. Mater. Sci. **55**, 1092–1106 (2020).